Biomaterials Science

PAPER

View Article Online
View Journal

Cite this: DOI: 10.1039/c8bm01632a

Systemic administration of enzyme-responsive growth factor nanocapsules for promoting bone repair†

Hongzhao Qi, ‡[a,b] Lijun Yang,‡[c] Xueping Li,‡[a] Xiaolei Sun,[a,d] Jin Zhao,[a] Xin Hou,[a] Zhaoyang Li, [a] Xubo Yuan, *[a] Zhenduo Cui[a] and Xianjin Yang*[a]

Accelerating the healing of bone fractures by local delivery of growth factors possessing osteoinductive activity has been extensively demonstrated. Unfortunately, for some complex clinical fractures, such as osteoporotic vertebral compression fracture, it is not possible to adopt such a strategy because of access restrictions. Systemic administration of growth factors is considered to be an appropriate alternative method due to its easy operability and precise spatiotemporal compatibility at fracture sites. But this therapy method was hampered by the poor *in vivo* stability, inefficient distribution at the fracture site and potential side effects of growth factors. To address these challenges, we conceived a systemic delivery platform of growth factors based on nanocapsules, taking advantage of the unique physiological character of bone fracture, *i.e.*, the malformed blood vessels and the over-expression of matrix metalloproteinases (MMPs). In this work, bone morphogenetic protein-2 (BMP-2), 2-(methacryloyloxy)ethyl phosphorylcholine (MPC) and the bisacryloylated VPLGVRTK peptide were respectively used as the model growth factor, monomer, and MMP-cleavable crosslinker. Nanocapsules were formed by *in situ* free radical polymerization on the surface of BMP-2 with MPC and peptides. The structure and function of BMP-2 were well maintained during the preparation process. BMP-2 nanocapsules (n(BMP-2)) were of uniform small size (~30 nm) possessing a long circulation time (half-life is ~48 h) and could be passively targeted to the fracture site through malformed blood vessels after systemic administration. Once accumulated at the fracture site, the shells of nanocapsules could be degraded by MMP and thus BMP-2 was released. Animal experiments proved that n(BMP-2) showed a better ability of bone repair than native BMP-2. In addition, n(BMP-2) showed a much lower inflammatory irritation. The results demonstrated that the systemic administration of growth factor nanocapsules could enhance their *in vivo* stability and fracture site delivery efficiency, realizing the efficient repair of a bone fracture. This rational delivery system may expand the bone repair types which can be administered with growth factors. Furthermore, the concept of taking advantage of the malformed vascular structure to deliver drugs potentially inspires researchers for the therapy of other diseases, especially sudden disease (such as cerebral hemorrhage).

Received 15th December 2018,
Accepted 20th January 2019

DOI: 10.1039/c8bm01632a

rsc.li/biomaterials-science

Introduction

Poorly healed fractures leading to prolonged hospitalization and significant morbidity have seriously affected the lives of patients.[1] To promote the repair of these fractures, growth factors, such as bone morphogenetic protein (BMP),[2,3] fibroblast growth factor (FGF),[4,5] and transforming growth factor-β (TGF-β),[6] have been delivered to fracture sites to stimulate bone formation. The mainstream way of growth factor administration, to date, is local delivery, mainly including local release from implant scaffolds and direct local injection.[7] For example, Nisarg J. Shah *et al.* used a polyelectrolyte multilayer coating on a biodegradable poly(lactic-*co*-glycolic acid) support membrane to deliver BMP-2 and platelet-derived growth factor-BB (PDGF-BB) for rapid bone repair.[8] Ludmila Luca *et al.* injected a biopolymer chitosan/β-TCP composite hydrogel loaded with 150 μg recombinant human BMP-2 to a 15 mm critical-size defect in the radius of a rabbit to demonstrate suc-

[a]*Tianjin Key Laboratory of Composite and Functional Materials, School of Materials Science and Engineering, Tianjin University, Tianjin 300072, China. E-mail: xbyuan@tju.edu.cn, xjyang@tju.edu.cn*
[b]*Institute for Translational Medicine, Qingdao University, Qingdao 266021, China*
[c]*College of Materials Science and Engineering, Qingdao University of Science and Technology, Qingdao 266042, China*
[d]*Department of Orthopaedics, Tianjin Hospital, Tianjin 300211, China*
†Electronic supplementary information (ESI) available. See DOI: 10.1039/c8bm01632a
‡These authors contributed equally to this work.

cessful osteoinduction.[9] The local delivery of growth factors is simple and efficient. However, the application of implant scaffolds is only suitable for specific fractures which have implantable space. As an example, two FDA-approved implant products based on BMPs are respectively used for the treatment of open tibia fractures and tibia long bone non-union because these fracture sites have ample space for the implantation of scaffolds.[10] Wataru Saito *et al.* also proved that implantable products were often difficult to place into metaphyseal fracture sites because of access restrictions.[11] In addition, for some complex clinical fractures, such as comminuted fracture and tiny fracture, it is difficult to realize the local injection of growth factors since these fractures don't have an exact or detectable location. In a word, local delivery of growth factors is only applied to specific bone injury models. Therefore, to expand the application of growth factors, it is necessary to develop a universal delivery method.

Systemic administration of growth factors is an appropriate way due to its easy operability and precise spatiotemporal compatibility at fracture sites. For example, systemic infusion of FGF-1 and TGF-β has been applied for bone regeneration successfully.[12,13] However, this feasible method was neglected over the past 20 years. This is mainly because of the short half-lives, inefficient accumulation at the fracture site and potential side effects of native growth factors.[14,15] In addition, the relatively simple bone injury models in fundamental research can be satisfied by the local delivery of growth factors further weakening the enthusiasm of researchers for the exploitation of a new administration method. Nanotechnology has been used to improve the *in vivo* deficiency of proteins. To take an example, Ming Wang *et al.* exploited a kind of protein–lipidoid nanocomplex realizing the efficient delivery of cytotoxic proteins for the suppression of tumor growth in a murine breast cancer model.[16] By far, however, few researchers have taken advantage of nanotechnology to systemically deliver growth factors for bone repair. Actually, physiological characteristics of the bone injury site provide conditions for nanotechnology-mediated systemic delivery of growth factors. At the early stage of bone injury, such as the hematoma process, the vasculature is ruptured and leaky, similar to the characteristics of the vascular system in the tumor site, facilitating the accumulation of nano-carriers.[17] Furthermore, vascular endothelial growth factor (VEGF) which is over-expressed in hematoma would disrupt vascular barrier function resulting in the improvement of vascular permeability.[18] Therefore, nanotechnology-mediated systemic delivery of growth factors for bone repair is technically feasible.

In addition, the early stage is critical for bone repair providing physiological feasibility. It has been proved that during the early stage of bone injury, the specific nature of fundamental processes initiates bone regeneration by stimulating the migration of mesenchymal stem cells, fibroblasts, and endothelial cells, as well as immune cells such as macrophages, driving the formation of soft callus and further processes.[19] As an example, removal of the fracture hematoma between days 2 and 4 as well as repeated hematoma debridement on days 1 and 2 resulted in delayed or non-union.[20] So the early intervention by systemic administration of growth factors facilitates the improvement of bone repair.

In this study, BMP-2 was chosen as the model growth factor. It is reasonable to improve bone repair by the application of BMP-2 at the early stage of bone injury since BMP-2 is the initiator of the endogenous bone repair response.[21] In addition, BMP-2 is a central regulator in the complex network of multiple BMPs.[22] To effectively deliver BMP-2 to fracture sites, we conceived a kind of nanocapsule. As illustrated in Scheme 1, the BMP-2 nanocapsules (denoted as n(BMP-2)) were synthesized by *in situ* polymerization on the BMP-2 surface with a 2-(methacryloyloxy)ethyl phosphorylcholine (MPC) monomer and matrix metalloproteinase (MMP) cleavable peptide crosslinker. The as-formed PMPC shells could efficiently stabilize BMP-2 and resist the non-specific adsorption of plasma proteins onto nanocapsules, prolonging the circulation time of n(BMP-2) and facilitating their accumulation within fracture sites through leaky blood vessels. The crosslinkers were specifically degraded by MMP (mainly MMP-2 and

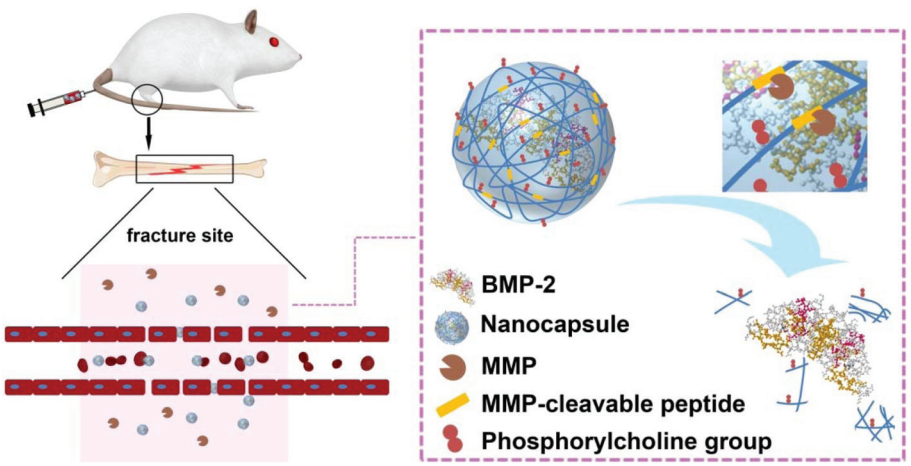

Scheme 1 Schematic illustration of enzyme-responsive BMP-2 nanocapsules (n(BMP-2)) and their systemic delivery for bone repair.

MMP-9). These MMPs were largely secreted into the extracellular matrix to degrade proteins during the bone repair process, while their content in normal tissues and blood was low.[23] This unique enzyme-responsive capability, therefore, stabilized the nanocapsules under physiological conditions, yet allowed the degradation of the polymer shells to release BMP-2 at the fracture sites. Taking advantage of these nanocapsules, we successfully realized the systemic administration of BMP-2 for promoting the repair of rat tibia fracture, providing a new alternative way for the repair of bone injury and expanding the bone repair types which can be administered with growth factors.

Experimental

Materials and reagents

All chemical reagents used were of analytical reagent grade and purchased from Sigma unless otherwise indicated. BMP-2 was purchased from Shanghai Rebone Biomaterials Co., Ltd. Peptide was purchased from ChinaPeptides. Phenyl-Sepharose CL-4B was obtained from Solarbio. An ALP ELISA kit and a BCA protein assay Kit were purchased from Beyotime. hUMSCs (human umbilical mesenchymal stem cells) and RAW 264.7 cells (mouse leukemic monocyte macrophage cell line) were purchased from Shanghai Zhong Qiao Xin Zhou Biotechnology Co., Ltd.

Synthesis and characteristics of n(BMP-2)

BMP-2 was dissolved using 20 mM phosphate buffers (PBS) in an ice-bath. *N*-(3-Aminopropyl) methacrylamide (APM), 2-methacryloyloxyethyl phosphorylcholine (MPC) and cross-linkers (bisacryloylated VPLGVRTK peptide) were added to the BMP-2 solution with stirring sequentially. The choice of this type of peptide was for two reasons. The amino group exists in both ends of the peptides facilitating their bisacryloylation. In addition, the middle portion of peptides was MMP-sensitive. Free-radical polymerization was initiated by adding ammonium persulfate (APS) and 10% *N*,*N*,*N*′,*N*′-tetramethylethylenediamine (TEMED) into the reaction solution. The final concentration of BMP-2 was adjusted to 1 mg mL^{-1} with PBS. The final molar ratio of BSA : APM : MPC : APS : TEMED was 1 : 300 : 4000 : 500 : 500 : 500. The polymerization was allowed to proceed for 120 min in a nitrogen atmosphere at 4 °C. The synthesized nanocapsules were purified by passing through a hydrophobic interaction column (Phenyl-Sepharose CL-4B) and dialyzed against PBS. To test the synthesis of n(BMP-2) using agarose gel electrophoresis, BMP-2 should be labeled with FITC previously and the preparation was the same as the above process.

The size and zeta potential of n(BMP-2) were measured using dynamic light scattering (DLS, BI-90Plus, Brookhaven Instruments Ltd, USA), and the samples were analyzed in triplicate. The morphology was assessed using a high-resolution transmission electron microscope (TEM, Jem-2100F, JEOL Ltd, Japan), and samples were stained with 2% phosphotungstic acid before observations.

The enzyme-responsive release of n(BMP-2)

The nanocapsule solution (1 mg mL^{-1}) was incubated with or without IV collagenase (2.0 μM) for 30 minutes at 37 °C, respectively. The degradation kinetics of the nanocapsules was quantified using the scattering light intensity ratio I/I_0 by DLS at selected time points, where I_0 represents the scattering light intensity of initial nanocapsules and I represents the time-dependent scattering light intensity of nanocapsules. Each test was repeated three times.

The structure detection of BMP-2 released from nanocapsules

To test the structural integrity of BMP-2 released from nanocapsules, the primary and secondary structures of the released BMP-2 were characterized. n(BMP-2) was firstly incubated with IV collagenase (2.0 μM) for 4 h at 37 °C and then the solution was dialyzed (molecular cut-off of 14 000 Da) overnight at 4 °C against 20 mM PBS to obtain the released BMP-2. The size of native BMP-2 and released BMP-2 was measured using dynamic light scattering. Each test was repeated six times. Native BMP-2 and released BMP-2 were heated for 5 min at 95 °C and analyzed *via* SDS-PAGE. Gel running electrophoresis was conducted for 2 h on 10% acrylamide gels with a 5% stacking gel at 120 V. The gels were run until the tracking dye had just exited the gel and then were stained with Coomassie blue brilliant R-250. In addition, Circular Dichroism (CD) analysis was performed on a spectrophotometer (Model J-810, Jasco, Tokyo, Japan). Native BMP-2 and released BMP-2 were prepared at 0.2 mg mL^{-1}. Measurements were collected at 37 °C over the wavelength range of 250–190 nm.

The activity test of BMP-2 released from nanocapsules

The hUMSCs were plated in six-well plates at a density of 5×10^4 cells per well. When the cells reached approximately 70% confluence, they were incubated with native BMP-2 and released BMP-2 (100 μg mL^{-1}). After 2 days of culture with DF-12 growth medium containing 10% heat-inactivated fetal bovine serum, cells were washed and extracted in cold RIPA lysis buffer containing Tris-HCl (50 nM, pH 8.0), NaCl (150 nM), Triton X-100 (1%), sodium deoxycholate (0.5%), SDS (0.1%) and a protease inhibitor [PMSF (1 mM), leupeptin (1 mg ml^{-1}), aprotinin (1 mg ml^{-1})]. The proteins were separated by 10% acrylamide gel electrophoresis and transferred to a PVDF membrane. After blocking for 1 h in 10% skimmed milk at room temperature, membranes were incubated overnight at 4 °C with antibodies to pSMAD1/5/8 (Merck Millipore, AB3848-I) and pERK (Merck Millipore, 05-797R). The following day, membranes were washed three times with TBST and were incubated with HRP-conjugated secondary antibody (Merck Millipore, AP510P) for 1 h at room temperature. Immunoreactive bands were visualized with the ECL detection system (Amersham; Arlington Heights, IL).

The osteogenic effect of BMP-2 released from nanocapsules

The hUMSCs were plated in six-well plates at a density of 5×10^4 cells per well. When the cells reached approximately 70%

confluence, they were incubated with BMP-2, n(BMP-2) and n(BMP-2) treated with IV collagenase at a final BMP-2 concentration of 100 μg mL^{-1}, the group with no treatment was set as a control group. Then, three days later, the DF-12 growth medium containing 10% heat-inactivated fetal bovine serum was replaced with an induction medium that contained 100 nM dexamethasone, 50 μg mL^{-1} ascorbic acid, and 10 mM β-glycerophosphate. The induction medium was changed every three days. The ALP expression of hUMSCs on day 7 was quantified by using the ELISA kit and on day 14 was checked by ALP staining. The mineralization of the hUMSCs was detected by Alizarin red staining on day 21 after induction. All samples were analyzed in triplicate.

The enzymatic degradation specificity of n(BMP-2)

The nanocapsule solution (1 mg mL^{-1}) was incubated with or without trypsin (2.0 μM) for 24 h at 37 °C, respectively. The scattering light intensity ratio (I/I_0) of samples was detected by DLS, where I_0 represents the scattering light intensity of the initial nanocapsules and I represents the scattering light intensity of nanocapsules after treatment. Each test was repeated three times.

Protein adsorption assay and phagocytosis studies

10 μL of PBS (negative control), BMP-2 (0.1 mg mL^{-1}) and n(BMP-2) (0.1 mg mL^{-1}) were mixed with 30 μL of mouse whole serum and incubated in a shaker at 37 °C for 30 min, respectively. After incubation, samples were filtered and washed with PBS three times with centrifugal filtration (molecular weight cut-off, MW = 100 kDa) to remove any unadsorbed serum proteins. After reconstituting with 50 μL of PBS, the amount of BMP-2 in each sample was measured using an ELISA kit. To better quantify the amount of adsorbed serum proteins, specific amounts of native BMP-2 were added to samples to ensure identical BMP-2 concentration. Finally, the amount of protein adsorbed was determined by measuring the overall protein concentration of each sample using BCA assays. Each test was repeated three times.

To evaluate the phagocytosis of n(BMP-2), RAW 264.7 cells with a density of 1×10^4 cells per well were seeded on eight-chamber slides and cultured overnight at 37 °C. Then cells were cultured for 4 h with fresh culture media in the presence of native BMP-2 as well as n(BMP-2) labeled with FITC (1 ml, 100 μg ml^{-1}) respectively. In addition, the native BMP-2 and n(BMP-2) had been pre-incubated with mouse serum treated at 37 °C for 30 min. After 4 h incubation, the cells were washed twice with PBS and fixed with methanol for 10 min. Following PBS washing, cells were labeled with DAPI for 5 min and imaged using an Olympus IX81 microscope.

To quantify the phagocytosis of n(BMP-2), RAW 264.7 cells with a density of 1×10^5 cells per well were seeded in 6-well plates and then incubated with native BMP-2 and n(BMP-2) (100 μg ml^{-1}) for 4 h. Next, the cells were harvested using trypsin-EDTA treatment followed by centrifugation and repeated washing in PBS. Fluorescence-activated cell sorting (FACS) was employed to count FITC positive cells within 1 h. Finally, 10 000 cells were counted and analyzed by measuring the signal from the FITC channel. Each test was repeated three times.

The blood circulation of n(BMP-2)

To test the blood clearance of n(BMP-2), healthy female SD rats were separated into two groups (native BMP-2 and n(BMP-2) groups), with 3 rats in each group. The solution of FITC-labeled BMP-2 and n(BMP-2) was single-dose injected *via* the tail vein (0.5 mg per kg body weight). The injections were well tolerated and no adverse effects were recorded during the observation period. All experimental protocols were conducted within Tianjin Medical University's guidelines for animal research and were approved by the Institutional Animal Care and Use Committee. At selected time points, blood was collected through the tail cut. Blood was centrifuged (5000 rpm, 10 min, 4 °C) and the fluorescence of the supernatant was tested. Fluorescence measurements were performed on a fluorescence spectrofluorometer.

The inflammation test of n(BMP-2)

Healthy female SD rats were randomly separated into seven groups with 3 rats in each group. Each group of rats was respectively injected with PBS, 0.2 mg of BMP-2, 1 mg of BMP-2, 5 mg of BMP-2, 0.2 mg of n(BMP-2), 1 mg of n(BMP-2) and 5 mg of n(BMP-2). After one day of injection, blood was collected through the tail cut and was centrifuged (5000 rpm, 10 min, 4 °C). Inflammatory markers in serum were quantified by using ELISA kits.

Biodistribution and bone injury targeting ability of n(BMP-2)

To study the accumulation efficiency of n(BMP-2) at the bone injury site, the rat tibial defect model was generated in SD rats. Six-week-old female SD rats were anesthetized with an intraperitoneal injection of 6% sodium pentobarbital. The animals were placed in the supine position on a heating pad to maintain their body temperature. After shaving and disinfecting the hind limb, a 2 cm incision through the skin was made on the proximal area of the tibia to expose the tibia. A 2 mm diameter round cortical and medullary defect was created using a dental drill under constant irrigation with 0.9% saline. One day after surgery, the rats were randomly divided into 3 groups, with 3 rats in each group. Two groups were respectively injected with Cy5.5-labeled BMP-2 and n(BMP-2) (1 mg per kg body weight) by the tail vein and one group was injected with the same volume of PBS as a control. The bio-distribution and the ability for targeting bone injury sites of native BMP-2 and n(BMP-2) were studied by using a IVIS imaging system. After observation, rats were sacrificed and the liver, spleen, kidney and broken tibia were taken for the qualitative and quantitative determination of fluorescence intensity. In addition, the bio-distribution of samples in rats with different times of tibial injury was also tested.

The bone repair efficiency of n(BMP-2)

The rat model of tibia injury was prepared according to the above method. Rats were randomly divided into three groups

and each group had ten rats. Two groups were respectively injected with native BMP-2 and n(BMP-2) (1 mg per kg body weight) by the tail vein and one group was injected with the same volume of PBS as a control. The samples were injected every other day for a total of five times. At selected time points, rats were euthanized to obtain defect sites. Three-dimensional microfocus X-ray microcomputed tomography (micro-CT) imaging was performed on specimens using a cone-beam micro-CT system (YXLON X-RAY, Germany). Samples from each experimental group at each time point were fixed in 4% paraformaldehyde solution in PBS and scanned through 360° with a rotation step of 0.5° at a spatial resolution of 21 μm at 80 kV, and 3D images were re-digitized with a 16-bit data format, proportional to the measured attenuation coefficients of the voxels. Bone reconstruction was created with standardized thresholds and morphometric parameters. Bone volume fraction (BV/TV; %) was measured using analysis software provided with the instrument. For histochemical analysis, harvested bones were fixed in 4% paraformaldehyde solution in PBS overnight and embedded into paraffin. Sections were stained with HE and Masson. A light microscope (TE2000U, Nikon, Japan) was used to view the sections.

The test of ectopic osteogenesis

The rat model of tibia injury was prepared according to the above method. Rats were randomly divided into three groups and each group had six rats. Two groups were respectively injected with native BMP-2 and n(BMP-2) (1 mg per kg body weight) by the tail vein and one group was injected with the same volume of PBS as a control. The samples were injected every other day for a total of five times. After eight weeks, rats were observed using X-rays and muscular tissue near the bone injury site was tested using HE staining.

Results and discussion

The preparation process of n(BMP-2) is shown in Fig. 1A. APM and MPC were used as monomers and the bisacryloylated VPLGVRTK peptide was the crosslinker. These monomers and the crosslinker would aggregate around BMP-2 at 4 °C relying on the electrostatic interaction and hydrogen-bond interaction.[24] APS and TEMED triggered the polymerization of monomers and the crosslinker to *in situ* form n(BMP-2).

The appropriate molar ratio of MPC to BMP-2 for the preparation of nanocapsules was tested. As shown in Fig. 1B, the overwhelming majority of BMP-2 could not be capsulated when the molar ratio was lower than 2000 : 1. This result indicated that there was a lower limit of MPC dosage for the capsulation of BMP-2. However, when the molar ratio was higher than 6000 : 1, a large part of BMP-2 was not released from nanocapsules, demonstrating that there was an upper limit of MPC dosage for the enzyme-responsive release of BMP-2 from nanocapsules. This may be because lots of MPC could efficiently inhibit the adsorption of the enzyme on nanocapsules. Sho Sakata *et al.* have proved that the zwitterionic polymer brush layer exhibited no significant interaction force with proteins and suppressed protein adsorption.[25] So to avoid the formation of non-degradable nanocapsules, a moderate amount of MPC should be adopted. The final molar ratio of MPC to BMP-2 was determined to be 4000 : 1 since BMP-2 was well capsulated and the resulting n(BMP-2) could be efficiently degraded under this condition. The morphology of n(BMP-2) was a regular spherical shape with a uniform diameter of 30 ± 5 nm (Fig. 1C). Consistent with the TEM observation, the dynamic light scattering (DLS) measurement showed that the mean diameter of n(BMP-2) was ~30 nm (Fig. 1D). As a kind of acidic protein, BMP-2 possessed electronegativity with a mean zeta potential of −18 mV in the physiological state, while the mean zeta potential of n(BMP-2) was nearly 0 mV because of the shielding effect of the MPC-based polymer shell (Fig. 1E). Elvin Blanco *et al.* have proved that nanoparticles with a high surface charge and large particle size were phagocytized more efficiently by the macrophages.[26] Approaches for escaping the phagocytic uptake included maintaining the particle size less than 150 nm and keeping the zeta potential below 15 mV. Therefore, the above results demonstrated that nanocapsules were potentially excellent delivery vectors for BMP-2 because of their regular spherical structure and appropriate size and zeta potential.

To verify the enzyme-responsive release ability of n(BMP-2), the size variation of n(BMP-2)s after incubation with IV collagenase which shared the same protein cleavage site (VPL↓GVRTK) with MMP (mainly MMP-2 and MMP-9) was measured.[27] The initial light scattering intensity of n(BMP-2) was I_0 and I was used to represent their light scattering intensity at different measurement time points. The light scattering intensity of n(BMP-2) was stable in 30 minutes without the incubation of IV collagenase. In contrast, it quickly decreased after incubation with IV collagenase (Fig. 2A). The reduction of light scattering intensity was because of the enzyme-responsive degradation of n(BMP-2) since the light scattering intensity of small particles was much lower than that of large particles.[28] This result indicated that BMP-2 could be rapidly released from nanocapsules under the action of the enzyme.

To confirm the integrity of BMP-2 released from nanocapsules, the size of native BMP-2 and released BMP-2 was compared (Fig. 2B). The diameter of released BMP-2 was similar to that of native BMP-2 implying the integrity of the primary structure of BMP-2. As shown in Fig. 2C (the insert picture), the band position of native BMP-2 was basically the same as that of released BMP-2. Their similar molecular weight further proved the above conclusion. In addition, the Circular Dichroism (CD) analysis of native BMP-2 and released BMP-2 (Fig. 2C) indicated that the secondary structure of BMP-2 was not destroyed. These results demonstrated that the primary and secondary structures of BMP-2 were complete during the preparation process of nanocapsules.

BMP-receptor interactions trigger the phosphorylation of SMAD1/5/8. The phosphorylated SMAD1/5/8 forms complexes with Co-SMAD that are translocated to the nucleus.[29] In addition, ERK1/2 pathways are also involved in BMP signal-

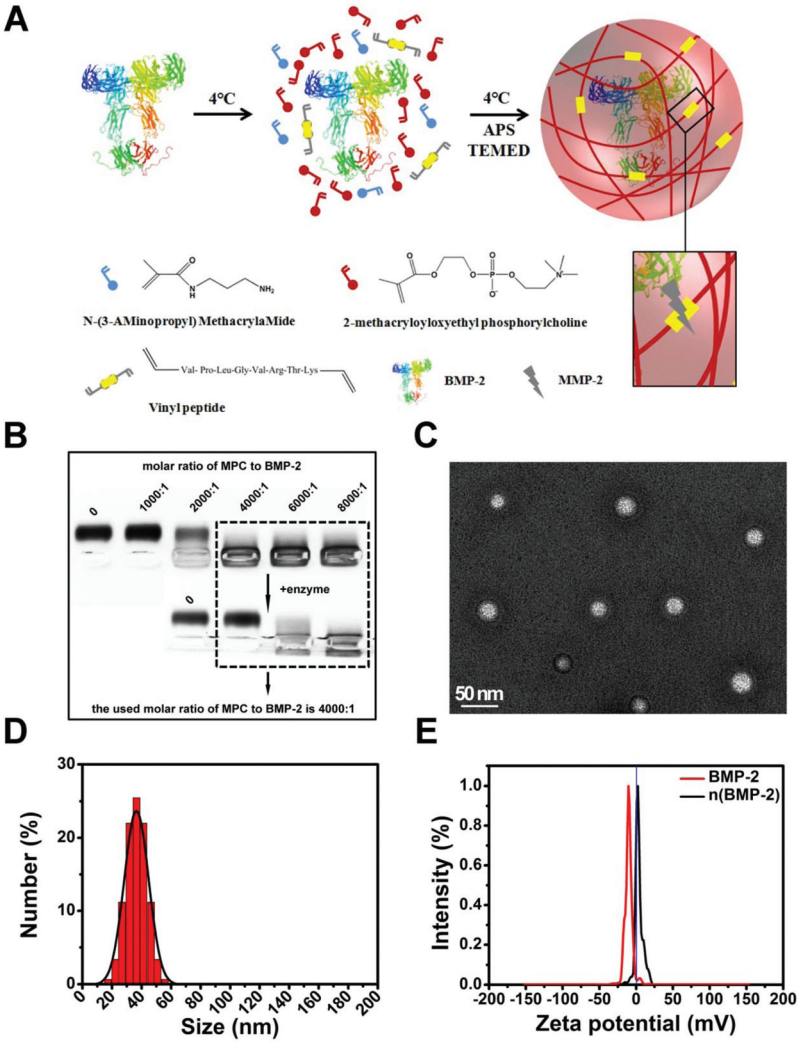

Fig. 1 (A) The synthesis mechanism of enzyme-responsive BMP-2 nanocapsules (n(BMP-2)); (B) agarose gel electrophoresis of n(BMP-2) which was synthesized at different molar ratios of MPC to BMP-2 and was treated with the enzyme; (C) representative TEM image of n(BMP-2); (D) the hydrodynamic size distribution of n(BMP-2); (E) the zeta potential of native BMP-2 and n(BMP-2).

ing.[30] The ability of native BMP-2 and released BMP-2 to phosphorylate SMAD1/5/8 and ERK was examined by WB analysis (Fig. 2D). The result showed that native BMP-2 and released BMP-2 both induced the phosphorylation of SMAD1/5/8 and ERK. The gray value of the native BMP-2 band was similar to that of released BMP-2 indicating the similar activity of native BMP-2 and released BMP-2. To further prove this conclusion, the alkaline phosphatase (ALP) activity of mesenchymal stem cells (MSCs) treated with native BMP-2 and n(BMP-2) was tested. As shown in Fig. 3A, n(BMP-2) didn't enhance the ALP expression of MSCs compared with native BMP-2. This may be because BMP-2 could not be released from nanocapsules, depriving their binding potential to MSCs. However, n(BMP-2) pretreated with IV collagenase dramatically enhanced the ALP expression of MSCs. Furthermore, ALP staining (Fig. 3B) and Alizarin red staining (Fig. 3C) of MSCs were performed. At day 14 after treatment, ALP staining was increased in the groups of native BMP-2 and n(BMP-2) incubated with IV collagenase and Alizarin red staining confirmed more calcium deposition in these groups at day 21. These results proved that the activity of BMP-2 released from nanocapsules was still well retained.

To test the enzymatic degradation specificity of n(BMP-2), the light scattering intensity of n(BMP-2) which was incubated with trypsin was monitored. After 30 minutes incubation of trypsin, almost no change of the light scattering intensity of n(BMP-2) was observed compared with that of initial n(BMP-2) (Fig. 3D). We had proved that the light scattering intensity of n(BMP-2) would be rapidly reduced when they were degraded. Therefore, n(BMP-2) could not be degraded by trypsin which had a different protein cleavage site to MMP. In addition, Alizarin red staining of MSCs incubated with n(BMP-2) and trypsin-treated n(BMP-2) was performed (the insert picture of Fig. 3D). A very low amount of calcium deposition was detected in the two groups because nanocapsules could not be

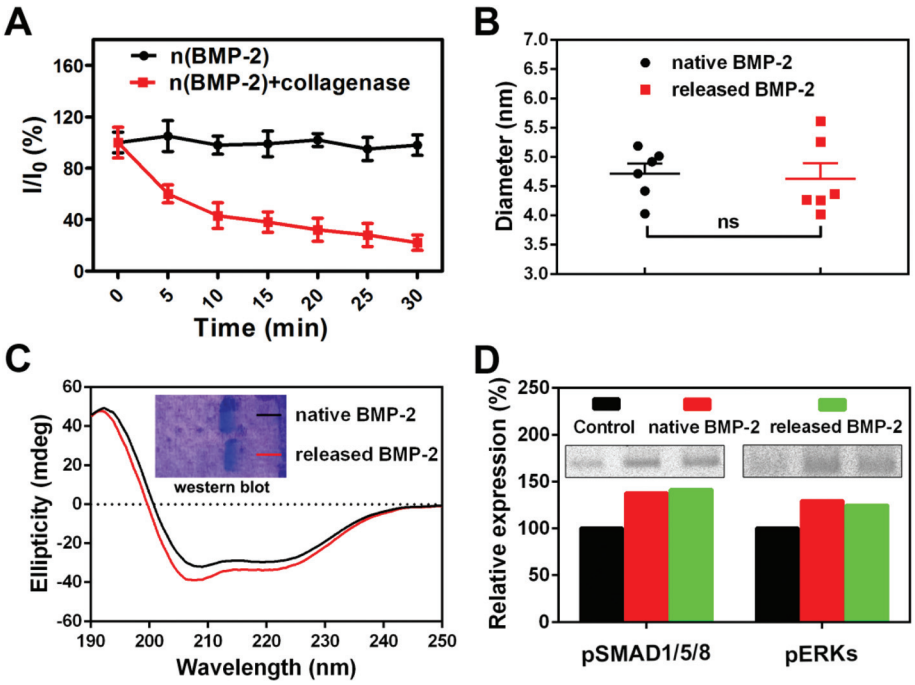

Fig. 2 (A) Degradation kinetics of n(BMP-2) in PBS with or without IV collagenase treatment measured by relative scattering light intensity; (B) the diameter of native BMP-2 and BMP-2 released from nanocapsules; (C) the Circular Dichroism (CD) analysis of native BMP-2 and released BMP-2, the insert picture shows the western blot analysis of native BMP-2 and released BMP-2; (D) the relative expression of the phosphorylation of SMAD1/5/8 and ERK in MSCs, the insert picture shows the result of western blot analysis.

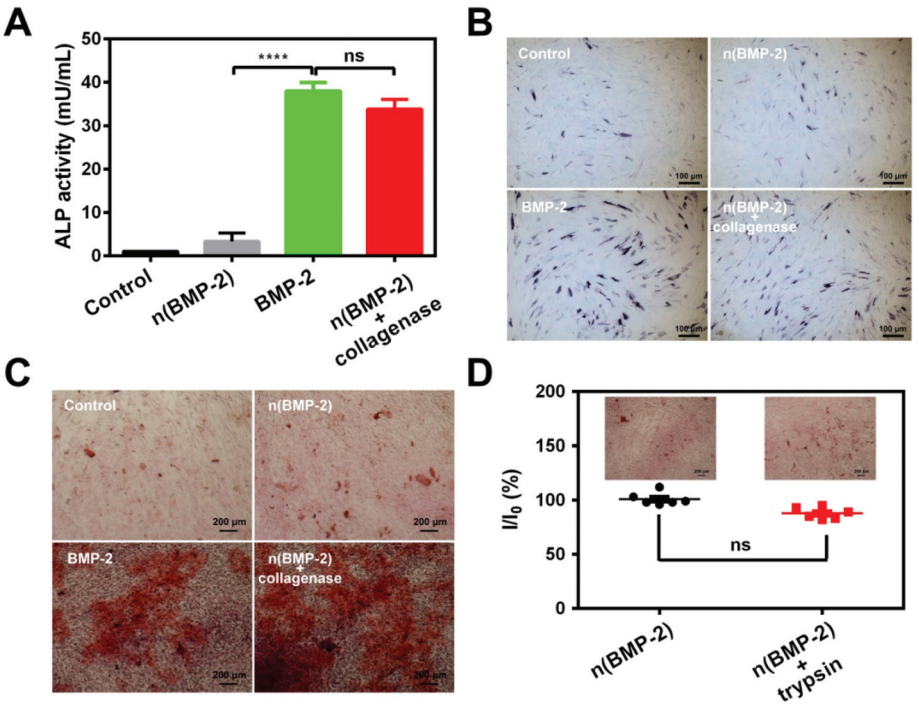

Fig. 3 (A) The expression of alkaline phosphatase (ALP) activity of MSCs incubated with native BMP-2 and n(BMP-2) (****$P < 0.0001$); (B) ALP staining of MSCs performed at day 14 of osteogenic differentiation; (C) alizarin red staining was performed at day 21 of osteogenic differentiation to visualize calcium nodule accumulation in MSCs; (D) the relative scattering light intensity of n(BMP-2) and trypsin-treated n(BMP-2), the insert picture shows alizarin red staining of MSCs incubated with n(BMP-2) and trypsin-treated n(BMP-2).

degraded by trypsin. These results indicated that n(BMP-2) were degraded by specific enzymes which were capable of degrading MMP sensitive peptides.

During the past few decades, actually, systemic administration of growth factors for bone repair was ignored mainly because of the low efficiency and potential side effects. After systemic administration, growth factors would be degraded by proteases easily resulting in low bioavailability.[31] Even when avoiding the degradation of the enzyme, the survival would distribute in other tissues besides bone injury sites. For example, BMP-2 would accumulate in the liver and other organs of the reticuloendothelial system since BMP-2 was a known chemoattractant for lymphocytes, monocytes, and macrophages.[32,33] These off-targeted growth factors potentially caused inflammation.[34] Here the enzymatic degradation specificity of nanocapsules could dramatically enhance the bioavailability and reduce the potential side effects of growth factors.

Nanocapsules efficiently prevented protein adsorption on BMP-2. As shown in Fig. S1,† 1 mg of native BMP-2 adsorbed ~0.4 mg of serum proteins obviously higher than that adsorbed on n(BMP-2). The current concept was that the presence of the protein corona had an impact on the presentation of nanoparticles to the immune cells and macrophages.[35] Therefore, due to the reduction of adsorbed serum proteins, the macrophage uptake of n(BMP-2) was dramatically decreased. Few fluorescence signals of n(BMP-2) were detected in their cytoplasm (Fig. 4A). But native BMP-2 was captured by macrophages massively. The result of flow cytometry showed that the macrophage uptake efficiency of native BMP-2 was ~27.24% at 100 μg mL^{-1}, which was much higher than that of n(BMP-2) (Fig. 4B). But it should be noted that the polymer shell of nanocapsules could not completely inhibit protein adsorption and macrophage uptake since nanocapsules were designed to be endowed with the ability of enzyme-responsive degradation.

The adsorption of serum proteins and the macrophage uptake affect the *in vivo* circulation of native BMP-2 and n(BMP-2). The half-life time of native BMP-2 was less than 30 minutes. In contrast, nanocapsules could dramatically prolong the circulation time of BMP-2 to ~48 hours (Fig. 4C). The prolonged *in vivo* retention of BMP-2 would enhance their bioavailability. In addition, the enzymatic degradation specificity of nanocapsules could avoid the rapid release of BMP-2 in normal tissues, reducing their potential side effects.

Inflammation results in a significant host of side effects of BMP-2 implantation. For example, the FDA released a black box warning for BMP-2 use owing to the recognized risk of cervical spine swelling and death in 2008.[36] To test the inflammatory response of the systemic administration of BMP-2, the concentration of inflammation markers in rat serum was determined by using ELISA (Fig. 4D). Similar to local delivery,

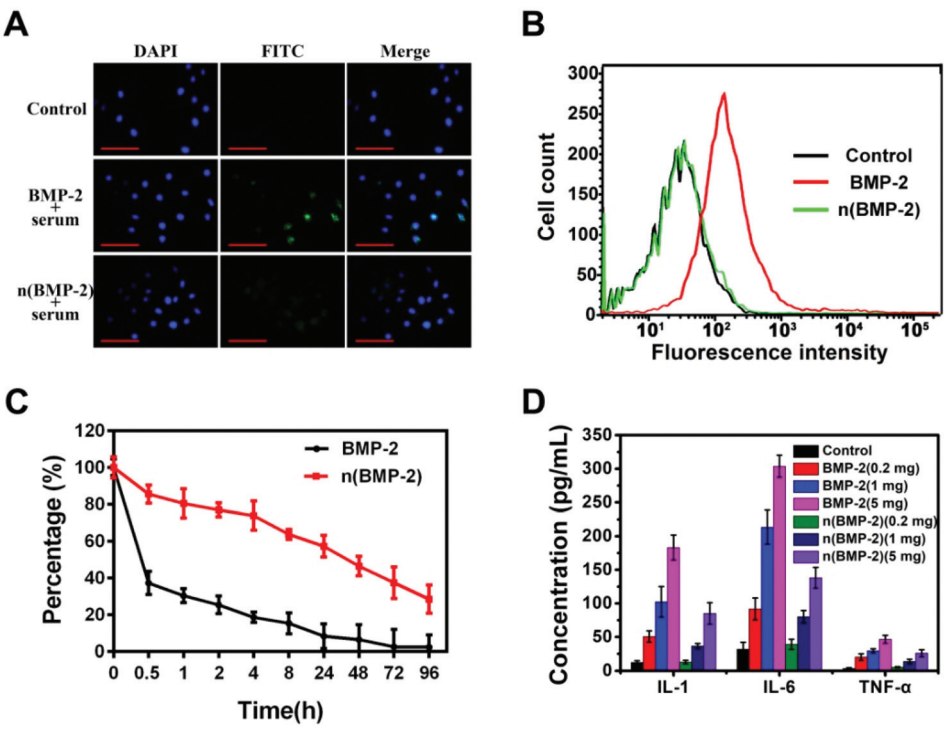

Fig. 4 (A) Fluorescence images of RAW 264.7 mouse macrophages after incubating with native BMP-2 or n(BMP-2) for 4 h, native BMP-2 and n(BMP-2) were labeled with FITC and were pre-incubated with mouse serum at 37 °C for 30 min, the scale bar was 200 μm; (B) quantitative fluorescence intensity from FACS analysis of RAW 264.7 mouse macrophages after incubating with native BMP-2 or n(BMP-2) for 4 h; (C) the circulation time of native BMP-2 and n(BMP-2) which were labeled with FITC; (D) the concentration of inflammation markers in rat serum was determined by using an ELISA kit.

the systemic administration of BMP-2 also caused inflammation. The more the injection dose of BMP-2 was, the more serious the inflammation was. Compared with native BMP-2, the same amount of n(BMP-2) showed a much lower inflammatory irritation. When injecting 0.2 mg of n(BMP-2), there were no detectable inflammation markers. Therefore, this injection dose was chosen as the therapeutic dose in the following research. These results demonstrated that nanocapsules could dramatically reduce the inflammatory response of BMP-2.

The accumulation efficiency of n(BMP-2) at the bone injury site was investigated using a SD rat with a tibia fracture. After 24 hours of intravenous injection, native BMP-2 could be accumulated at the bone injury site relying on their intrinsic passive targeting ability. However, due to their rapid elimination in circulation, the accumulation efficiency of native BMP-2 was low. Nanocapsules dramatically enhanced the accumulation of BMP-2 at the bone injury site (Fig. 5A). The *ex vivo* fluorescence imaging of the rat major organs indicated that nanocapsules greatly reduced the elimination of BMP-2 by the liver, spleen, and kidney (Fig. 5B). In our opinion, the accumulation of growth factors or growth factor nanocapsules at the injury site was the result of the interaction of external and internal factors. Jianzhong Hu *et al.* proved that trauma led to a serious volumetric collapse of the microvascular structure.[37] In addition, a wide array of inflammatory mediators at the bone injury site, such as VEGF, could disrupt the vascular barrier function to enhance the vascular permeability. These external and internal factors collectively caused the vascular malformation, facilitating the leakage of biomacromolecules from the blood circulation system. This phenomenon was similar to the EPR effect in the tumor site. We believed that taking advantage of the malformed vascular structure to deliver drugs could be applied to many diseases, especially sudden diseases, such as cerebral hemorrhage.

We also tested the accumulation efficiency of n(BMP-2) at the bone injury site after the different times of tibia fracture. n(BMP-2) could be accumulated at the bone injury site even after 7 days of tibia fracture (Fig. 5C). This feature facilitated multiple administrations of growth factors during treatment. It should be noted that the accumulation efficiency was gradually decreased because of the remodeling of damaged blood vessels.

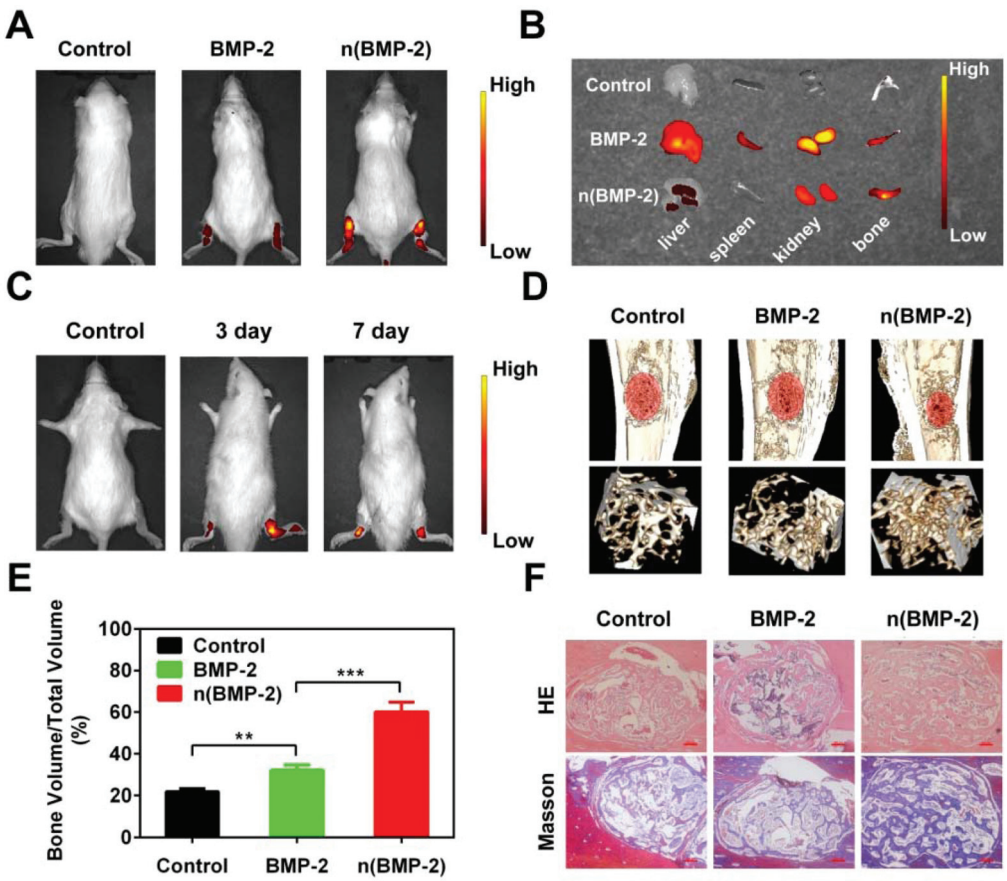

Fig. 5 (A) *In vivo* fluorescence images of a rat with tibial injury after intravenous injection of native BMP-2 and n(BMP-2); (B) the distribution of BMP-2 and n(BMP-2) in main tissues and the tibial injury site after intravenous injection of BMP-2 and n(BMP-2); (C) *in vivo* fluorescence images of mice with different times of tibial injury after intravenous injection of n(BMP-2); (D) micro-CT images of representative rat tibias after two weeks of therapy; (E) semi-quantitative analysis of the volume of bone tissue per volume of total tissue (BV/TV) after two weeks of therapy (**P < 0.01, ***P < 0.001); (F) HE and Masson staining analysis of bone formation in each group after two weeks of therapy, the scale bar was 200 μm.

Actually, it needs the synergistic effect of multiple growth factors during natural bone repair.[38] To simulate the process, researchers usually load multiple growth factors on the scaffold to sequentially release them. For example, Julianne L. Holloway *et al.* used hyaluronic acid hydrogels to deliver SDF-1 and BMP-2 for bone repair.[39] Compared with local delivery, the systemic administration can spatially and temporally realize the combined application of growth factors. As an example, we can first deliver vascular endothelial growth factor (VEGF) to induce angiogenesis and then deliver transforming growth factor-β (TGF-β) to recruit stem cells. The new blood vessels can provide a pathway for stem cells and supply oxygen and nutrients. In addition, we can also sequentially deliver three or more growth factors through systemic administration. With the help of nanocapsules, the accumulation efficiency of the sequential delivery of growth factors can be dramatically enhanced. However, it should be noted that the delivered growth factors should work mainly in the early stage of bone injury since the accumulation efficiency of nanocapsules was gradually decreased.

The *in vivo* efficiency of n(BMP-2) for bone repair was measured using rat tibia fracture of 2 mm in diameter. Micro-CT images were collected to evaluate newly formed bone volume and connectivity. At two weeks, the fracture site was most significantly bridged with bone in the n(BMP-2) group. In contrast, the native BMP-2 group had less bone binding and slower healing (Fig. 5D). Micro-CT quantitative analysis showed that the bone volume/total volume of the n(BMP-2) group was ~60.13% which was apparently higher than that of the native group (~32.09%) (Fig. 5E). The trabecular spacing of the n(BMP-2) group was also much smaller than that of the native BMP-2 group (Fig. S2†). In addition, HE staining and Masson staining were further performed to measure the effects of n(BMP-2) on bone repair (Fig. 5F). The new bone area, which was composed of a more trabeculae meshwork and some lamellar bone, of the n(BMP-2) group at two weeks was significantly higher than that of the native BMP-2 group. These results confirmed that nanocapsules enhanced the bone repair efficiency of BMP-2.

To verify the side effects of n(BMP-2), we observed the bone repair at eight weeks. The results of micro-CT (Fig. S3†), HE staining and Masson staining (Fig. S4†) indicated there was no difference in bone repair between the control group and n(BMP-2) group. In addition, we used X-ray irradiation to determine whether n(BMP-2) would cause ectopic osteogenesis. The image showed that no bone was formed in other rat tissues of the n(BMP-2) group (Fig. S5†). This may be because of the low injection dosage since native BMP-2 also did not cause ectopic osteogenesis. Furthermore, muscles of the fracture site were examined by HE staining (Fig. S6†). Muscle cells of all groups were normal further confirming the bio-safety of n(BMP-2).

In our opinion, compared with the local delivery of BMP-2, systemic administration shows the lower potential of the ectopic bone formation. During the local delivery process, the ectopic bone formation is associated with BMP-2 leakage outside the implant site. Leakage can occur into the epidural space and lead to root compression of nerves by ectopic bone impingement. Systemic administration can realize the precise spatiotemporal compatibility of BMP-2 at fracture sites, avoiding their improper or redundant leakage. In addition, the enzyme-responsive release characteristic of nanocapsules further reduces the ectopic bone formation potential of BMP-2.

Conclusions

Enzyme-responsive nanocapsules successfully realized the systemic administration of BMP-2 for promoting the repair of rat tibia fracture, verifying the feasibility of nanotechnology-mediated systemic delivery of growth factors for bone repair. Here we provide a new alternative way for the repair of bone injury and expand the bone repair types which can be administered with growth factors. Furthermore, taking advantage of malformed vascular structure for drug delivery can be applied to other diseases, such as cerebral hemorrhage. This may inspire other researchers to exploit new treatment methods for sudden diseases.

Conflicts of interest

The authors declare no competing financial and nonfinancial interests.

Acknowledgements

This work was supported by grants from the National Nature Science Foundation of China (No. 31370970, 51673144 and 31600769), the Natural Science Foundation of Tianjin City (No. 18JCYBJC18300) and the Medical and Health Technology Development Program of Shandong Province (2017WS490).

References

1 S. Murali, B. Rai, C. Dombrowski, J. Lee, Z. Lim, D. Bramono, L. Ling, T. Bell, S. Hinkley, S. Nathan, J. Hui, H. Wong, V. Nurcombe and S. Cool, *Biomaterials*, 2013, **34**, 5594–5605.
2 C. V. Rahman, D. Ben-David, A. Dhillon, G. Kuhn, T. W. Gould, R. Müller, F. R. Rose, K. M. Shakesheff and E. Livne, *J. Tissue Eng. Regener. Med.*, 2014, **8**, 59–66.
3 J. P. Issa, M. Gonzaga, B. G. Kotake, C. de Lucia, E. Ervolino and M. Iyomasa, *Clin. Oral Implants Res.*, 2016, **27**, 558–566.
4 H. Furuya, Y. Tabata and K. Kaneko, *Tissue Eng., Part A*, 2014, **20**, 1531–1541.
5 T. Yoshida, H. Miyaji, K. Otani, K. Inoue, K. Nakane, H. Nishimura, A. Ibara, A. Shimada, K. Ogawa and E. Nishida, *J. Periodontal Res.*, 2015, **50**, 265–273.

6 P. Bhattacharjee, D. Naskar, T. K. Maiti, D. Bhattacharya and S. C. Kundu, *J. Colloid Interface Sci.*, 2016, **472**, 16–33.
7 R. Agarwal and A. J. García, *Adv. Drug Delivery Rev.*, 2015, **94**, 53–62.
8 N. J. Shah, M. N. Hyder, M. A. Quadir, N. M. D. Courchesne, H. J. Seeherman, M. Nevins, M. Spector and P. T. Hammond, *Proc. Natl. Acad. Sci. U. S. A.*, 2014, **111**, 12847–12852.
9 L. Luca, A. L. Rougemont, B. H. Walpoth, L. Boure, A. Tami, J. M. Anderson, O. Jordan and R. Gurny, *J. Biomed. Mater. Res., Part A*, 2011, **96**, 66–74.
10 K. W. H. Lo, B. D. Ulery, K. M. Ashe and C. T. Laurencin, *Adv. Drug Delivery Rev.*, 2012, **64**, 1277–1291.
11 W. Saito, K. Uchida, M. Ueno, O. Matsushita, G. Inoue, N. Nishi, T. Ogura, S. Hattori, H. Fujimaki and K. Tanaka, *J. Biomed. Mater. Res., Part A*, 2014, **102**, 3049–3055.
12 C. Dunstan, R. Boyce, B. Boyce, I. Garrett, E. Izbicka, W. Burgess and G. Mundy, *J. Bone Miner. Res.*, 1999, **14**, 953–959.
13 M. Machwate, E. Zerath, X. Holy, M. Hott, D. Godet, A. Lomri and P. J. Marie, *J. Clin. Invest.*, 1995, **96**, 1245–1253.
14 Y. Liu, T. Nelson, B. Cromeens, T. Rager, J. Lannutti, J. Johnson and G. E. Besner, *Biomaterials*, 2016, **103**, 150–159.
15 Z. Wang, Z. Wang, W. W. Lu, W. Zhen, D. Yang and S. Peng, *NPG Asia Mater.*, 2017, **9**, e435.
16 M. Wang, K. Alberti, S. Sun, C. L. Arellano and Q. Xu, *Angew. Chem., Int. Ed.*, 2014, **53**, 2893–2898.
17 Y. Zhang, Z. Jia, H. Yuan, A. Dusad, K. Ren, X. Wei, E. V. Fehringer, P. E. Purdue, A. Daluiski and S. R. Goldring, *Pharm. Res.*, 2016, **33**, 1959–1971.
18 S. M. Weis and D. A. Cheresh, *Nature*, 2005, **437**, 497–504.
19 P. Kolar, T. Gaber, C. Perka, G. N. Duda and F. Buttgereit, *Clin. Orthop. Relat. Res.*, 2011, **469**, 3118–3126.
20 P. Kolar, K. Schmidt-Bleek, H. Schell, T. Gaber, D. Toben, G. Schmidmaier, C. Perka, F. Buttgereit and G. N. Duda, *Tissue Eng., Part B*, 2010, **16**, 427–434.
21 K. Tsuji, A. Bandyopadhyay, B. D. Harfe, K. Cox, S. Kakar, L. Gerstenfeld, T. Einhorn, C. J. Tabin and V. Rosen, *Nat. Genet.*, 2006, **38**, 1424–1429.
22 C. M. Edgar, V. Chakravarthy, G. Barnes, S. Kakar, L. C. Gerstenfeld and T. A. Einhorn, *Bone*, 2007, **40**, 1389–1398.
23 K. B. S. Paiva and J. M. Granjeiro, *Arch. Biochem. Biophys.*, 2014, **561**, 74–87.
24 J. Ge, D. Lu, J. Wang, M. Yan, Y. Lu and Z. Liu, *J. Phys. Chem. B*, 2008, **112**, 14319–14324.
25 S. Sakata, Y. Inoue and K. Ishihara, *Langmuir*, 2015, **31**, 3108–3114.
26 E. Blanco, H. Shen and M. Ferrari, *Nat. Biotechnol.*, 2015, **33**, 941–951.
27 J. Wen, S. M. Anderson, J. Du, M. Yan, J. Wang, M. Shen, Y. Lu and T. Segura, *Adv. Mater.*, 2011, **23**, 4549–4553.
28 T. Zheng, S. Bott and Q. Huo, *ACS Appl. Mater. Interfaces*, 2016, **8**, 21585–21594.
29 D. P. Brazil, R. H. Church, S. Surae, C. Godson and F. Martin, *Trends Cell Biol.*, 2015, **25**, 249–264.
30 G. Sánchez-Duffhues, C. Hiepen, P. Knaus and P. ten Dijke, *Bone*, 2015, **80**, 43–59.
31 S. Zhang and H. Uludağ, *Pharm. Res.*, 2009, **26**, 1561–1580.
32 N. S. Cunningham, V. Paralkar and A. Reddi, *Proc. Natl. Acad. Sci. U. S. A.*, 1992, **89**, 11740–11744.
33 A. Valentin-Opran, J. Wozney, C. Csimma, L. Lilly and G. E. Riedel, *Clin. Orthop. Relat. Res.*, 2002, **395**, 110–120.
34 J. N. Zara, R. K. Siu, X. Zhang, J. Shen, R. Ngo, M. Lee, W. Li, M. Chiang, J. Chung, J. Kwak, B. M. Wu, K. Ting and C. Soo, *Tissue Eng., Part A*, 2011, **17**, 1389–1399.
35 F. Chen, G. Wang, J. I. Griffin, B. Brenneman, N. K. Banda, V. M. Holers, D. S. Backos, L. Wu, S. M. Moghimi and D. Simberg, *Nat. Nanotechnol.*, 2017, **12**, 387–393.
36 A. W. James, G. LaChaud, J. Shen, G. Asatrian, V. Nguyen, X. Zhang, K. Ting and C. Soo, *Tissue Eng., Part B*, 2016, **22**, 284–297.
37 J. Z. Hu, T. D. Wu, T. Zhang, Y. F. Zhao, J. Pang and H. B. Lu, *J. Neurosci. Methods*, 2012, **204**, 150–158.
38 D. H. Kempen, L. B. Creemers, J. Alblas, L. Lu, A. J. Verbout, M. J. Yaszemski and W. J. Dhert, *Tissue Eng., Part B*, 2010, **16**, 551–566.
39 J. L. Holloway, H. Ma, R. Rai, K. D. Hankenson and J. A. Burdick, *Macromol. Biosci.*, 2015, **15**, 1218–1223.